

Shadow Ansatz for the Many-Fermion Wave Function in Scalable Molecular Simulations on Quantum Computing Devices

Yuchen Wang, Irma Avdic and David A. Mazziotti^{1,*}

¹*Department of Chemistry and The James Franck Institute,
The University of Chicago, Chicago, Illinois 60637, USA*

(Dated: Submitted August 8, 2024)

Here we show that shadow tomography can generate an efficient and exact ansatz for the many-fermion wave function on quantum devices. We derive the shadow ansatz—a product of transformations applied to the mean-field wave function—by exploiting a critical link between measurement and preparation. Each transformation is obtained by measuring a classical shadow of the residual of the contracted Schrödinger equation (CSE), the many-electron Schrödinger equation (SE) projected onto the space of two electrons. We show that the classical shadows of the CSE vanish if and only if the wave function satisfies the SE and, hence, that randomly sampling only the two-electron space yields an exact ansatz regardless of the total number of electrons. We demonstrate the ansatz’s advantages for scalable simulations—fewer measurements and shallower circuits—by computing H_3 on simulators and a quantum device.

Introduction.—Simulating many-body systems is one of the most promising applications for near-term quantum computers [1–5]. Various algorithms that demonstrate a potential quantum advantage over classical ones have been proposed over time, including phase estimation [6–10], imaginary time evolution [11–14] and the variational quantum eigensolver (VQE) [15–20], with the VQE receiving significant attention due to its shallow circuit depth and adaptive ansatz form. It is widely acknowledged that the chosen VQE ansatz has a profound impact on the performance characteristics of the algorithm, including circuit depth, convergence speed, and result accuracy [19, 21–24]. For example, the chemistry-inspired unitary coupled cluster ansatz [25–34] suffers from a large parameter space [35] while the hardware-efficient ansatz [17, 24] tailors the parametrization to the quantum device but is limited by the barren plateau phenomenon [36–38].

In this Letter, we derive an efficient and exact ansatz for the many-fermion wave function on quantum devices by combining concepts from shadow tomography [39–70] and reduced density matrix theory [71–75]. We obtain each transformation in the shadow ansatz—a product of transformations applied to the mean-field reference—by measuring a classical shadow of the residual of the contracted Schrödinger equation (CSE) [76–81], the many-electron Schrödinger equation (SE) projected onto the space of two electrons. Selecting each classical shadow with respect to a randomly sampled one-electron basis, we show, completely covers the quantum two-electron space with respect to both measurement and preparation. Moreover, we prove that the classical shadows of the CSE vanish if and only if the wave function satisfies the SE and, hence, the shadow ansatz is exact regardless of the quantum system’s total number of electrons. Advantages of the shadow ansatz, relative to solving the

CSE or its anti-Hermitian part with full tomography [82–90], include fewer measurements and shallower circuits.

We first present the theory of the shadow ansatz, followed by quantum simulation results for the linear H_3 chain using a noiseless simulator and a noisy 127-qubit IBM quantum computer. We examine the differences and advantages of the shadow ansatz compared to the existing ansatz and showcase its ability to reduce computational costs for scalable simulation on near-term quantum devices.

Theory.— Let us first briefly recall CSE theory. Consider the SE for an N -electron system

$$(\hat{H} - E)|\Psi\rangle = 0, \quad (1)$$

where \hat{H} is the Hamiltonian operator and $|\Psi\rangle$ is the wave function. Projecting the SE onto the two-electron space yields the CSE [76–81]

$$\langle\Psi|\hat{a}_i^\dagger\hat{a}_j^\dagger\hat{a}_l\hat{a}_k(\hat{H} - E)|\Psi\rangle = 0, \quad (2)$$

where \hat{a}_i^\dagger and \hat{a}_i are the fermionic creation and annihilation operators for orbital i . While the SE clearly implies CSE, we can prove the reverse that the CSE implies the variance that implies the SE [76, 91], demonstrating that the CSE and SE share a common set of energetically non-degenerate pure-state solutions.

Iterative solution of the CSE suggests an exact product ansatz for the wave function [86, 92, 93]

$$|\Psi_{n+1}\rangle = \prod_{q=0}^n e^{-\eta_q \hat{R}_q^\dagger} |\Psi_0\rangle, \quad (3)$$

where

$$\hat{R}_q = \sum_{ijkl} {}^2 R_q^{ij;kl} \hat{a}_i^\dagger \hat{a}_j^\dagger \hat{a}_l \hat{a}_k. \quad (4)$$

Descent along the gradient of the energy with respect to

* damazz@uchicago.edu

the wave function's parameters ${}^2R_n^{ij:kl}$ at the n^{th} iteration ($q = n$) occurs when these parameters equal the residual of the CSE. Hence, the gradient at a given iteration vanishes if and only if the CSE and thus, the SE are satisfied, proving the ansatz's exactness [92].

Here we exploit this connection by drawing inspiration from the theory of shadow tomography [39–70] to prepare a shadow ansatz, which enhances both state preparation and measurement with reduced circuit depth and measurement cost. Rather than directly projecting the SE onto the two-electron space, we project the SE onto a set of classical shadows ${}^2S_q^{ij}$ where each classical shadow is the diagonal (or classical) part of the two-electron space with respect to a given random unitary transformation \hat{U}_q of the orbitals

$${}^2S_q^{ij} = \langle \Psi | \hat{U}_q^\dagger \hat{a}_i^\dagger \hat{a}_j^\dagger \hat{a}_i \hat{a}_j \hat{U}_q (\hat{H} - E) | \Psi \rangle. \quad (5)$$

Each classical shadow of dimension r^2 where r is the number of spin orbitals is a subset of the CSE residual of dimension r^4 . Because there are r^2 linearly independent unitary transformations of the orbitals, connecting each of the diagonal orbitals to each of the off-diagonal orbitals, a set of $O(r^2)$ classical shadows of total dimension r^4 represents a shadow projection of the SE onto the two-electron space—a shadow CSE—that is equivalent to the CSE. Consequently, we have the following generalization of the exactness of the CSE: a wave function satisfies the shadow CSE if and only if it satisfies the SE.

Building upon the parallels between the shadow CSE and the CSE, we can define a shadow ansatz for the many-fermion wave function

$$|\Psi_{n+1}\rangle = \prod_{q=0}^n \left(\prod_{t=1}^M e^{-\eta_{qt} \hat{S}_{qt}^\dagger} \right) |\Psi_0\rangle, \quad (6)$$

where

$$\hat{S}_{qt} = \hat{U}_{qt} \left(\sum_{ij} {}^2S_{qt}^{ij} \hat{a}_i^\dagger \hat{a}_j^\dagger \hat{a}_i \hat{a}_j \right) \hat{U}_{qt}^\dagger. \quad (7)$$

Each of the M classical shadows in the n^{th} iteration is defined with respect to the n^{th} wave function, using a different random unitary transformation. In the limit that M approaches r^2 , the shadow ansatz effectively becomes the previously developed CSE ansatz in Eq. (3). The value of M can also be varied between iterations, allowing one to tune between the CSE ansatz and the single-shadow-per-iteration ($M = 1$) ansatz. Like the CSE ansatz, we can follow the energy gradient descent direction by setting the parameters at the n^{th} iteration to the M classical shadows of the CSE residual, as shown for one classical shadow in Eq. (5). Hence, the energy gradient at the n^{th} iteration vanishes if and only if the M classical shadows of the residual vanish. The shadow ansatz becomes exact if we continue its construction until $O(r^2)$ classical shadows of the CSE vanish, which implies

TABLE I. CQE algorithm that solves the ACSE with the shadow ansatz.

Algorithm: CQE with the shadow ansatz

Given $n = 0$ and convergence tolerance ϵ .

Choose initial wave function $|\Psi_0\rangle$.

Repeat until the residual is less than ϵ :

Step 1: Prepare $|\Lambda^\pm\rangle = e^{\pm i\delta H} |\Psi_n\rangle$.

Step 2: Measure M shadows with Eq. (9).

Step 3: Update $|\Psi_n\rangle$ from M shadows.

Step 4: Optimize energy with respect to η_{mt} .

Step 5: Set $n \leftarrow n + 1$.

the CSE and hence, the SE.

To implement the ansatz on quantum simulators or devices, we further split the classical shadow of the residual in Eq. (5) into its Hermitian and anti-Hermitian parts, displayed below as the anti-commutator and commutator respectively,

$$2 {}^2S_{qt}^{ij} = \langle \Psi_q | \{ \hat{U}_{qt}^\dagger \hat{a}_i^\dagger \hat{a}_j^\dagger \hat{a}_i \hat{a}_j \hat{U}_{qt} (\hat{H} - E) \} | \Psi_q \rangle + \langle \Psi_q | [\hat{U}_{qt}^\dagger \hat{a}_i^\dagger \hat{a}_j^\dagger \hat{a}_i \hat{a}_j \hat{U}_{qt}, \hat{H}] | \Psi_q \rangle. \quad (8)$$

The anti-Hermitian portion, known as the anti-Hermitian CSE (ACSE) [94–100], can be readily implemented via unitary transformations on quantum computers [84, 101]. While ACSE does not strictly imply the CSE [92], practical calculations on quantum simulators and devices show that, at least for the molecular systems explored, it converges to the energies and 2-RDMs from full configuration interaction (FCI) [82–90]. We note that, as shown in recent work [86], it is possible to implement the full residual and non-unitary transformation on quantum computers with dilation techniques [102, 103].

To obtain the classical shadow of the ACSE part of the residual in Eq. (8), we measure

$${}^2S_{qt}^{ij} = \frac{1}{2i\delta} (\langle \Lambda_q^+ | \hat{U}_{qt}^\dagger \hat{a}_i^\dagger \hat{a}_j^\dagger \hat{a}_i \hat{a}_j \hat{U}_{qt} | \Lambda_q^+ \rangle - \langle \Lambda_q^- | \hat{U}_{qt}^\dagger \hat{a}_i^\dagger \hat{a}_j^\dagger \hat{a}_i \hat{a}_j \hat{U}_{qt} | \Lambda_q^- \rangle) + O(\delta^2), \quad (9)$$

where $|\Lambda_q^\pm\rangle = e^{\pm i\delta H} |\Psi_q\rangle$ in which δ is the stepsize [101]. Table I and Fig. 1 summarize the iterative algorithm—a contracted quantum eigensolver (CQE)—that solves the ACSE with the shadow ansatz. In the results presented here, we form the unitary transformations \hat{U} from the tensor product of random single-qubit unitaries drawn from the single-qubit Clifford subgroup. Other choices for the unitary ensemble can be readily incorporated into the algorithm for future studies and potential improvements [43–45, 49].

The number of Pauli exponential terms in the proposed algorithm scales as $O(\alpha r^2)$, where α is the number of repetitive measurements and r is the number of orbitals, in which α has been shown to scale polylogarithmically with the system size [39]. Compared to the full 2-RDM

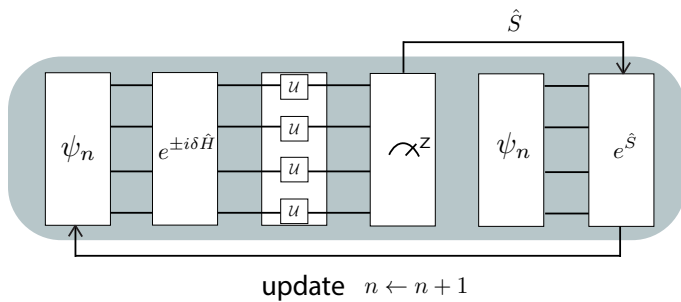


FIG. 1. A schematic representation of the CQE algorithm with the shadow ansatz.

tomography with an $O(r^4)$ cost, the shadow ansatz is advantageous in the number of measurements, and, even more importantly, since the ansatz directly utilizes the measurement outcomes, the improvement over conventional tomography is also manifested in the circuit depth.

Results—We use the CQE with the shadow ansatz to perform calculations on the linear molecule H_3 with equally spaced bond lengths on a noiseless six-qubit statevector simulator and the noisy 127-qubit IBM Cleveland device [104, 105]. We compute the spin sector $\langle \hat{S}_z \rangle = 1$ for H_3 with the Slater-type Gaussian orbital (STO-3G) basis set [106]. Electron integrals and FCI are computed with PySCF [107]. For the noiseless simulator, we use the Jordan-Wigner mapping [108, 109] to map the six spin-orbitals to six qubits. For IBM Cleveland, additional tapering techniques are used to map the Hamiltonian to three qubits. More details on the implementation can be found in the Supplemental Material (SM).

Figure 2 (a) illustrates the convergence of the CQE ground-state energy of H_3 to the FCI [110] wave function solution, as a function of the number M of shadows per iteration, on a noiseless simulator. The initial trial wave function is the normalized and unweighted sum of all possible spin-adapted Slater determinants to minimize the potential effect of the initial guess. All calculations show exact convergence to the FCI solution, even with the imposed randomized measurement. This shows that the shadow ACSE ansatz with as few as five shadows ($M = 5$) may be sufficient to converge rapidly to the FCI solution. The more shadows employed, the fewer iterations are needed for the convergence, which can be viewed as the shadow residual approaching the exact residual limit.

In Fig. 2 (b), we further compare the circuit depth of the shadow ansatz with different numbers M of shadows per iteration. The circuit depth is represented by the number of elementary Pauli exponential terms after first-order Trotterization. For a number of shadows fewer than 40, as more shadows are employed, the number of iterations decreases but the circuit depth remains approximately constant, suggesting a trade-off between the number of iterations and the number M of shadows per iteration. We also observe that once the number

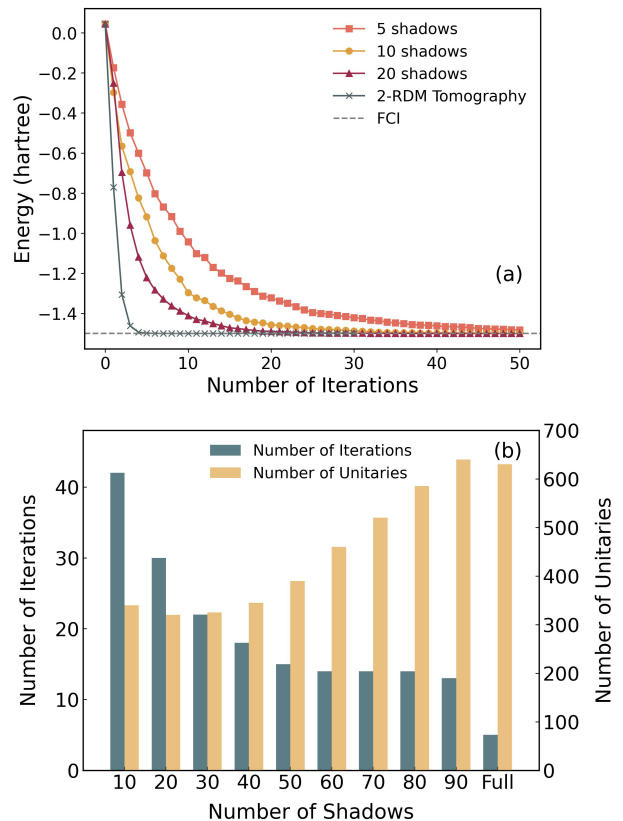


FIG. 2. Convergence data for the linear molecule H_3 with equal bond lengths of 0.7 Å. (a) As a function of the iteration number, the energies from the shadow ansatz with different numbers M of shadows are compared with the energy from the CSE ansatz with conventional 2-RDM tomography. (b) As a function of the number M of shadows per iteration, the number of iterations and the circuit depth, required to reach energy convergence within 1 mhartree, are compared.

M of shadows per iteration exceeds 40, further increasing M does not significantly accelerate the convergence, but instead increases the circuit depth, leading to two important conclusions. First, the number M of shadows employed to minimize the residual to a desired level of accuracy should not exceed an upper limit to maximize circuit efficiency. Second, provided that the number of shadows remains below the established upper limit, the distribution of shadows across iterations has a rather small impact on circuit depth. This flexibility allows for the dynamic manipulation of the shadow ansatz. It is also worth noting that the exact 2-RDM tomography leads to the fewest iterations but not the optimal circuit depth, which can be attributed to the fact that the residual from exact tomography usually contains many trivial terms that do not contribute significantly to the optimization direction.

Due to the decoherence effect prevalent on current quantum computers, it is necessary to maintain a low circuit depth for any practical algorithm. In previous work,

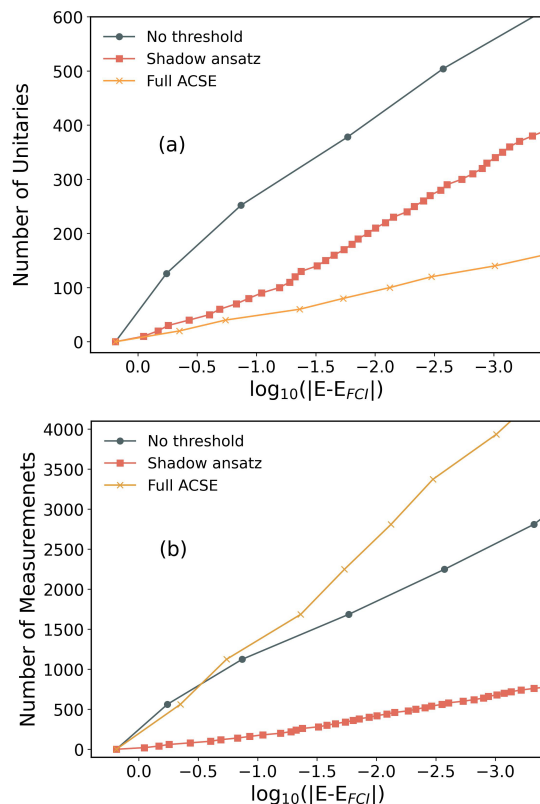


FIG. 3. (a) The number of accumulated unitaries and (b) the number of required measurements plotted against accuracy during optimization. The energy obtained from the full configuration interaction (or exact diagonalization) is denoted as E_{FCI} . 20 shadows are used per iteration. The number of measurements refers to the number of distinct circuits, which should be distinguished from the number of shots applied to each circuit reported in the SM.

we employed a threshold to filter small contributions from the residual. A straightforward implementation of this thresholding is to decompose the residual in the Pauli basis and filter the coefficients of the terms based on their magnitude, which creates a linear increase in circuit depth with respect to the number of iterations. The effect of thresholding is illustrated in Fig. 3 (a). Both the shadow ansatz and the conventional ACSE ansatz, after applying the threshold, achieve a significant reduction in circuit depth, measured in the number of unitaries, compared to the results with no applied thresholding. The conventional ACSE ansatz provides slightly better convergence with the number of unitaries than the shadow ansatz. However, concerning the number of measured circuits, shown in Fig. 3 (b), the shadow ansatz significantly outperforms the conventional ACSE ansatz. The threshold in conventional ACSE ansatz is performed in a post-selection of unitaries with designated measurement instructions, which means that we still measure much more information than needed. In contrast, the shadow

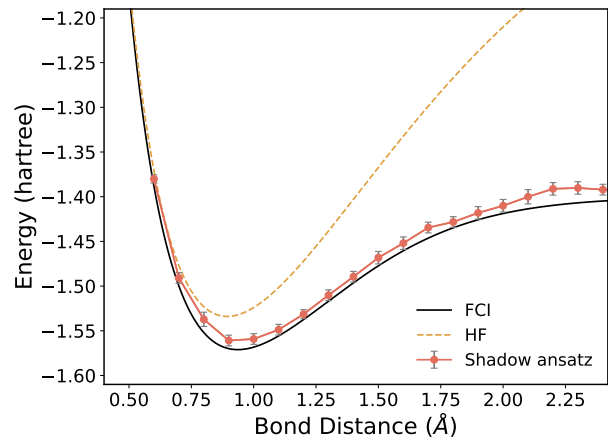


FIG. 4. The dissociation curve of linear H_3 obtained with Hartree-Fock (HF), full configuration interaction (FCI), and the shadow ansatz. The hydrogen atoms are kept equally spaced during bond stretching. The data point and error bar are plotted as mean value \pm standard deviation.

ansatz provides a protocol for thresholding in an “on-the-fly” manner with random sampling decreasing the number of measurements.

We examine the performance of the shadow ansatz on realistic quantum computers by performing the simulation of linear H_3 on the 127-qubit IBM Cleveland device [104]. The dissociation curves of H_3 , obtained from the Hartree-Fock (HF), full configuration interaction (FCI), and the shadow-ansatz methods are plotted in Fig. 4. Bond lengths are kept equally spaced upon dissociation. The curve from the initial HF trial wave function is indicated by the dashed lines. The shadow ansatz is able to capture the correlation energy from the HF guess, especially in the dissociated region where HF does not perform well due to its restriction to a single Slater determinant. The results obtained from shadow ansatz differ from FCI on average by approximately 16 mhartree, which is quite accurate given the degree of noise on the near intermediate-scale quantum (NISQ) computers.

Discussion and conclusions— Two challenges for the quantum simulation of many-electron quantum systems are: (i) measurement of observables and (ii) preparation of the wave function. Classical shadows—classical snapshots that collectively represent a quantum system—were developed to improve the efficiency of measurements in (i). Here we combine shadow tomography [39–70] with 2-RDM theory [71–75] to improve the preparation in (ii). Measuring the two-electron CSE—the projection of the many-electron SE onto the two-electron space—provides all the information necessary to construct an exact ansatz for the many-electron wave function [92]. The CSE from 2-RDM theory, therefore, provides a critical link between measurement and preparation. By combining the CSE with shadow tomography, we obtain a highly efficient exact ansatz—the shadow ansatz—in which the many-electron wave function is directly constructed from the

classical shadows of the CSE. Relative to full tomography, the shadow ansatz provides both a decrease in the circuit depth (when compared to the ACSE ansatz without thresholding) and a significant reduction in the number of measurements needed to construct the wave function. The improvements in efficiency have important implications for realizing scalable molecular simulations. Future work will explore further extensions and improvements of the shadow ansatz including the use of optimal

shadow tomography protocols beyond those implemented here.

Acknowledgments—D.A.M gratefully acknowledges the U.S. National Science Foundation Grant No. CHE-2155082 and the U.S. Department of Energy, Office of Basic Energy Sciences, Grant DE-SC0019215. I.A. gratefully acknowledges the NSF Graduate Research Fellowship Program under Grant No. 2140001. The views expressed are of the authors and do not reflect the official policy or position of IBM or the IBMQ team.

-
- [1] D. S. Abrams and S. Lloyd, Simulation of many-body fermi systems on a universal quantum computer, *Phys. Rev. Lett.* **79**, 2586 (1997).
- [2] Y. Cao, J. Romero, J. P. Olson, M. Degroote, P. D. Johnson, M. Kieferová, I. D. Kivlichan, T. Menke, B. Peropadre, N. P. Sawaya, *et al.*, Quantum chemistry in the age of quantum computing, *Chem. Rev.* **119**, 10856 (2019).
- [3] K. Head-Marsden, J. Flick, C. J. Ciccarino, and P. Narang, Quantum Information and Algorithms for Correlated Quantum Matter, *Chem. Rev.* **121**, 5 (2021).
- [4] S. McArdle, S. Endo, A. Aspuru-Guzik, S. C. Benjamin, and X. Yuan, Quantum computational chemistry, *Rev. Mod. Phys.* **92**, 015003 (2020).
- [5] R. Dutta, D. G. Cabral, N. Lyu, N. P. Vu, Y. Wang, B. Allen, X. Dan, R. G. Cortiñas, P. Khazaei, S. E. Smart, *et al.*, Simulating chemistry on bosonic quantum devices, arXiv preprint arXiv:2404.10214 [10.48550/arXiv.2404.10214](https://arxiv.org/abs/2404.10214) (2024).
- [6] D. S. Abrams and S. Lloyd, Quantum algorithm providing exponential speed increase for finding eigenvalues and eigenvectors, *Phys. Rev. Lett.* **83**, 5162 (1999).
- [7] A. Aspuru-Guzik, A. D. Dutoi, P. J. Love, and M. Head-Gordon, Simulated quantum computation of molecular energies, *Science* **309**, 1704 (2005).
- [8] J. Du, N. Xu, X. Peng, P. Wang, S. Wu, and D. Lu, Nmr implementation of a molecular hydrogen quantum simulation with adiabatic state preparation, *Phys. Rev. Lett.* **104**, 030502 (2010).
- [9] S. Paesani, A. A. Gentile, R. Santagati, J. Wang, N. Wiebe, D. P. Tew, J. L. O’Brien, and M. G. Thompson, Experimental bayesian quantum phase estimation on a silicon photonic chip, *Phys. Rev. Lett.* **118**, 100503 (2017).
- [10] A. Y. Kitaev, Quantum measurements and the Abelian Stabilizer Problem, arXiv [10.48550/arxiv.quant-ph/9511026](https://arxiv.org/abs/10.48550/arxiv.quant-ph/9511026) (1995), [quant-ph/9511026](https://arxiv.org/abs/10.48550/arxiv.quant-ph/9511026).
- [11] S. McArdle, T. Jones, S. Endo, Y. Li, S. C. Benjamin, and X. Yuan, Variational ansatz-based quantum simulation of imaginary time evolution, *npj Quantum Inf.* **5**, 75 (2019).
- [12] M. Motta, C. Sun, A. T. Tan, M. J. O’Rourke, E. Ye, A. J. Minnich, F. G. Brandao, and G. K.-L. Chan, Determining eigenstates and thermal states on a quantum computer using quantum imaginary time evolution, *Nat. Phys.* **16**, 205 (2020).
- [13] H. Kamakari, S.-N. Sun, M. Motta, and A. J. Minnich, Digital quantum simulation of open quantum systems using quantum imaginary-time evolution, *PRX Quantum* **3**, 010320 (2022).
- [14] T. Tsuchimochi, Y. Ryo, S. C. Tsang, and S. L. Ten-no, Multi-state quantum simulations via model-space quantum imaginary time evolution, *npj Quantum Information* **9**, [10.1038/s41534-023-00780-y](https://doi.org/10.1038/s41534-023-00780-y) (2023).
- [15] Y. Cao, A. Papageorgiou, I. Petras, J. Traub, and S. Kais, Quantum algorithm and circuit design solving the Poisson equation, *New J. Phys.* **15**, 013021 (2013).
- [16] A. Peruzzo, J. McClean, P. Shadbolt, M.-H. Yung, X.-Q. Zhou, P. J. Love, A. Aspuru-Guzik, and J. L. O’Brien, A variational eigenvalue solver on a photonic quantum processor, *Nature Commun.* **5**, 4213 (2014).
- [17] A. Kandala, A. Mezzacapo, K. Temme, M. Takita, M. Brink, J. M. Chow, and J. M. Gambetta, Hardware-efficient variational quantum eigensolver for small molecules and quantum magnets, *Nature* **549**, 242 (2017).
- [18] K. M. Nakanishi, K. Mitarai, and K. Fujii, Subspace-search variational quantum eigensolver for excited states, *Phys. Rev. Res.* **1**, 033062 (2019).
- [19] H. R. Grimsley, S. E. Economou, E. Barnes, and N. J. Mayhall, An adaptive variational algorithm for exact molecular simulations on a quantum computer, *Nat. Commun.* **10**, 3007 (2019).
- [20] H. L. Tang, V. Shkolnikov, G. S. Barron, H. R. Grimsley, N. J. Mayhall, E. Barnes, and S. E. Economou, qubit-adapt-vqe: An adaptive algorithm for constructing hardware-efficient ansätze on a quantum processor, *PRX Quantum* **2**, 020310 (2021).
- [21] K. Mitarai, T. Yan, and K. Fujii, Generalization of the output of a variational quantum eigensolver by parameter interpolation with a low-depth ansatz, *Phys. Rev. Appl.* **11**, 044087 (2019).
- [22] H. R. Grimsley, D. Claudino, S. E. Economou, E. Barnes, and N. J. Mayhall, Is the trotterized uccsd ansatz chemically well-defined?, *J. Chem. Theory Comput.* **16**, 1 (2019).
- [23] S. Sim, P. D. Johnson, and A. Aspuru-Guzik, Expressibility and entangling capability of parameterized quantum circuits for hybrid quantum-classical algorithms, *Adv. Quantum Technol.* **2**, 1900070 (2019).
- [24] R. D’Cunha, T. D. Crawford, M. Motta, and J. E. Rice, Challenges in the use of quantum computing hardware-efficient ansätze in electronic structure theory, *J. Phys. Chem. A* **127**, 3437 (2023).
- [25] R. J. Bartlett, S. A. Kucharski, and J. Noga, Alternative coupled-cluster ansätze ii. the unitary coupled-cluster method, *Chem. Phys. Lett.* **155**, 133 (1989).
- [26] J. Romero, R. Babbush, J. R. McClean, C. Hempel,

- P. J. Love, and A. Aspuru-Guzik, Strategies for quantum computing molecular energies using the unitary coupled cluster ansatz, *Quantum Sci. Technol.* **4**, 014008 (2018).
- [27] A. Anand, P. Schleich, S. Alperin-Lea, P. W. Jensen, S. Sim, M. Díaz-Tinoco, J. S. Kottmann, M. Degroote, A. F. Izmaylov, and A. Aspuru-Guzik, A quantum computing view on unitary coupled cluster theory, *Chem. Soc. Rev.* **51**, 1659 (2022).
- [28] S. Guo, J. Sun, H. Qian, M. Gong, Y. Zhang, F. Chen, Y. Ye, Y. Wu, S. Cao, K. Liu, *et al.*, Experimental quantum computational chemistry with optimized unitary coupled cluster ansatz, *Nat. Phys.* , 1 (2024).
- [29] Z. W. Windom, D. Claudino, and R. J. Bartlett, A new “gold standard”: Perturbative triples corrections in unitary coupled cluster theory and prospects for quantum computing, *J. Chem. Phys.* **160**, 214113 (2024).
- [30] A. Mitra, R. D’Cunha, Q. Wang, M. R. Hermes, Y. Alexeev, S. K. Gray, M. Otten, and L. Gagliardi, The Localized Active Space Method with Unitary Selective Coupled Cluster, arXiv 10.48550/2404.12927 (2024), 2404.12927.
- [31] J. Lee, W. J. Huggins, M. Head-Gordon, and K. B. Whaley, Generalized unitary coupled cluster wave functions for quantum computation, *J. Chem. Theory Comput.* **15**, 311 (2018).
- [32] M. R. Hoffmann and J. Simons, A unitary multiconfigurational coupled-cluster method: Theory and applications, *J. Chem. Phys.* **88**, 993–1002 (1988).
- [33] D. A. Fedorov, Y. Alexeev, S. K. Gray, and M. Otten, Unitary selective coupled-cluster method, *Quantum* **6**, 703 (2022).
- [34] S. G. Mehendale, B. Peng, N. Govind, and Y. Alexeev, Exploring parameter redundancy in the unitary coupled-cluster ansätze for hybrid variational quantum computing, *J. Phys. Chem. A* **127**, 4526–4537 (2023).
- [35] D. Wecker, M. B. Hastings, and M. Troyer, Progress towards practical quantum variational algorithms, *Physical Review A* **92**, 042303 (2015).
- [36] R. Wiersema, C. Zhou, Y. de Sereville, J. F. Carrasquilla, Y. B. Kim, and H. Yuen, Exploring entanglement and optimization within the hamiltonian variational ansatz, *PRX Quantum* **1**, 020319 (2020).
- [37] M. Cerezo, A. Sone, T. Volkoff, L. Cincio, and P. J. Coles, Cost function dependent barren plateaus in shallow parametrized quantum circuits, *Nature Commun.* **12**, 1791 (2021), 2001.00550.
- [38] C.-Y. Park, M. Kang, and J. Huh, *Hardware-efficient ansatz without barren plateaus in any depth* (2024).
- [39] S. Aaronson, Shadow tomography of quantum states, *SIAM J. Comput.* **49**, STOC18 (2020).
- [40] H.-Y. Huang, R. Kueng, and J. Preskill, Predicting many properties of a quantum system from very few measurements, *Nat. Phys.* **16**, 1050 (2020).
- [41] H.-Y. Huang, Learning quantum states from their classical shadows, *Nat. Rev. Phys.* **4**, 81 (2022).
- [42] A. Elben, S. T. Flammia, H.-Y. Huang, R. Kueng, J. Preskill, B. Vermersch, and P. Zoller, The randomized measurement toolbox, *Nat. Rev. Phys.* **5**, 9 (2023).
- [43] A. Zhao, N. C. Rubin, and A. Miyake, Fermionic partial tomography via classical shadows, *Phys. Rev. Lett.* **127**, 110504 (2021).
- [44] H. C. Nguyen, J. L. Bönsel, J. Steinberg, and O. Gühne, Optimizing shadow tomography with generalized measurements, *Phys. Rev. Lett.* **129**, 220502 (2022).
- [45] H.-Y. Hu, S. Choi, and Y.-Z. You, Classical shadow tomography with locally scrambled quantum dynamics, *Phys. Rev. Res.* **5**, 023027 (2023).
- [46] A. A. Akhtar, H.-Y. Hu, and Y.-Z. You, Scalable and flexible classical shadow tomography with tensor networks, *Quantum* **7**, 1026 (2023).
- [47] K. Wan, W. J. Huggins, J. Lee, and R. Babbush, Matchgate shadows for fermionic quantum simulation, *Commun. Math. Phys.* **404**, 629 (2023).
- [48] M. Ippoliti, Y. Li, T. Rakovszky, and V. Khemani, Operator relaxation and the optimal depth of classical shadows, *Phys. Rev. Lett.* **130**, 230403 (2023).
- [49] J. Helsen and M. Walter, Thrifty shadow estimation: Reusing quantum circuits and bounding tails, *Phys. Rev. Lett.* **131**, 240602 (2023).
- [50] C. Bertoni, J. Haferkamp, M. Hinsche, M. Ioannou, J. Eisert, and H. Pashayan, Shallow shadows: Expectation estimation using low-depth random clifford circuits, *Phys. Rev. Lett.* **133**, 020602 (2024).
- [51] B. Wu and D. E. Koh, Error-mitigated fermionic classical shadows on noisy quantum devices, *npj Quantum Inf.* **10**, 39 (2024).
- [52] K. Bu, D. E. Koh, R. J. Garcia, and A. Jaffe, Classical shadows with pauli-invariant unitary ensembles, *npj Quantum Inf.* **10**, 6 (2024).
- [53] B. Vermersch, A. Rath, B. Sundar, C. Branciard, J. Preskill, and A. Elben, Enhanced estimation of quantum properties with common randomized measurements, *PRX Quantum* **5**, 010352 (2024).
- [54] I. Avdic and D. A. Mazziotti, Fewer measurements from shadow tomography with N -representability conditions, *Phys. Rev. Lett.* **132**, 220802 (2024).
- [55] S. N. Hearth, M. O. Flynn, A. Chandran, and C. R. Laumann, Efficient Local Classical Shadow Tomography with Number Conservation, arXiv 10.48550/2311.09291 (2023), 2311.09291.
- [56] C. Gyurik, R. Molteni, and V. Dunjko, Limitations of measure-first protocols in quantum machine learning, arXiv 10.48550/2311.12618 (2023), 2311.12618.
- [57] S. Jerbi, C. Gyurik, S. C. Marshall, R. Molteni, and V. Dunjko, Shadows of quantum machine learning, arXiv 10.48550/2306.00061 (2023), 2306.00061.
- [58] L. Lewis, H.-Y. Huang, V. T. Tran, S. Lehner, R. Kueng, and J. Preskill, Improved machine learning algorithm for predicting ground state properties, *Nat. Commun.* **15**, 895 (2024).
- [59] B. O’Gorman, Fermionic tomography and learning, arXiv 10.48550/2207.14787 (2022), 2207.14787.
- [60] D. E. Koh and S. Grewal, Classical Shadows With Noise, *Quantum* **6**, 776 (2022), 2011.11580.
- [61] L. Coopmans, Y. Kikuchi, and M. Benedetti, Predicting Gibbs-State Expectation Values with Pure Thermal Shadows, *PRX Quantum* **4**, 010305 (2023), 2206.05302.
- [62] E. A. R. Guzman and D. Lacroix, Restoring symmetries in quantum computing using Classical Shadows, arXiv 10.48550/2311.04571 (2023), 2311.04571.
- [63] H. Jnane, J. Steinberg, Z. Cai, H. C. Nguyen, and B. Koczor, Quantum Error Mitigated Classical Shadows, *PRX Quantum* **5**, 010324 (2024), 2305.04956.
- [64] H.-Y. Hu, A. Gu, S. Majumder, H. Ren, Y. Zhang, D. S. Wang, Y.-Z. You, Z. Mineev, S. F. Yelin, and A. Seif, Demonstration of Robust and Efficient Quantum Property Learning with Shallow Shadows, arXiv

- 10.48550/arxiv.2402.17911 (2024), 2402.17911.
- [65] F. Truger, J. Barzen, F. Leymann, and J. Obst, Warm-Starting the VQE with Approximate Complex Amplitude Encoding, arXiv 10.48550/arxiv.2402.17378 (2024), 2402.17378.
- [66] A. Caprotti, J. Morris, and B. Dakić, Optimising quantum tomography via shadow inversion, arXiv 10.48550/arxiv.2402.06727 (2024), 2402.06727.
- [67] J. Majsak, D. McNulty, and M. Oszmaniec, A Simple and Efficient Joint Measurement Strategy for Estimating Fermionic Observables and Hamiltonians, arXiv 10.48550/arxiv.2402.19230 (2024), 2402.19230.
- [68] R. Levy, D. Luo, and B. K. Clark, Classical shadows for quantum process tomography on near-term quantum computers, *Phys. Rev. Research* **6**, 013029 (2024), 2110.02965.
- [69] S. Becker, N. Datta, L. Lami, and C. Rouze, Classical Shadow Tomography for Continuous Variables Quantum Systems, *IEEE Trans. Inf.* **70**, 3427 (2024), 2211.07578.
- [70] R. D. Somma, R. King, R. Kothari, T. O'Brien, and R. Babbush, Shadow Hamiltonian Simulation, arXiv 10.48550/arxiv.2407.21775 (2024), 2407.21775.
- [71] D. A. Mazziotti, ed., *Reduced-Density-Matrix Mechanics: With Application to Many-Electron Atoms and Molecules*, Advances in Chemical Physics, Vol. 134 (John Wiley & Sons, New York, 2007).
- [72] A. J. Coleman and V. I. Yukalov, *Reduced Density Matrices: Coulson's Challenge* (Springer, Berlin, 2000).
- [73] D. A. Mazziotti, Two-Electron Reduced Density Matrix as the Basic Variable in Many-Electron Quantum Chemistry and Physics, *Chem. Rev.* **112**, 244 (2012).
- [74] M. Piris, Global Natural Orbital Functional: Towards the Complete Description of the Electron Correlation, *Phys. Rev. Lett.* **127**, 233001 (2021), 2112.02119.
- [75] D. A. Mazziotti, Quantum Many-Body Theory from a Solution of the N -Representability Problem, *Phys. Rev. Lett.* **130**, 153001 (2023), 2304.08570.
- [76] D. A. Mazziotti, Contracted Schrödinger equation: Determining quantum energies and two-particle density matrices without wave functions, *Phys. Rev. A* **57**, 4219 (1998).
- [77] H. Nakatsuji and K. Yasuda, Direct determination of the quantum-mechanical density matrix using the density equation, *Phys. Rev. Lett.* **76**, 1039 (1996).
- [78] F. Colmenero and C. Valdemoro, Approximating q -order reduced density matrices in terms of the lower-order ones. ii. applications, *Phys. Rev. A* **47**, 979 (1993).
- [79] C. Valdemoro, L. Tel, and E. Pérez-Romero, The contracted Schrödinger equation: some results, *Adv. Quantum Chem.* **28**, 33 (1997).
- [80] D. A. Mazziotti, Pursuit of N -representability for the contracted Schrödinger equation through density-matrix reconstruction, *Phys. Rev. A* **60**, 3618 (1999).
- [81] D. A. Mazziotti, Variational method for solving the contracted Schrödinger equation through a projection of the n -particle power method onto the two-particle space, *J. Chem. Phys.* **116**, 1239 (2002).
- [82] S. E. Smart and D. A. Mazziotti, Quantum solver of contracted eigenvalue equations for scalable molecular simulations on quantum computing devices, *Phys. Rev. Lett.* **126**, 070504 (2021).
- [83] S. E. Smart, J.-N. Boyn, and D. A. Mazziotti, Resolving correlated states of benzyne with an error-mitigated contracted quantum eigensolver, *Phys. Rev. A* **105**, 022405 (2022).
- [84] S. E. Smart and D. A. Mazziotti, Many-fermion simulation from the contracted quantum eigensolver without fermionic encoding of the wave function, *Phys. Rev. A* **105**, 062424 (2022).
- [85] S. E. Smart and D. A. Mazziotti, Accelerated Convergence of Contracted Quantum Eigensolvers through a Quasi-Second-Order, Locally Parameterized Optimization, *J. Chem. Theory Comp.* **18**, 5286 (2022).
- [86] S. E. Smart and D. A. Mazziotti, Verifiably exact solution of the electronic Schrödinger equation on quantum devices, *Phys. Rev. A* **109**, 022802 (2024).
- [87] Y. Wang and D. A. Mazziotti, Electronic excited states from a variance-based contracted quantum eigensolver, *Phys. Rev. A* **108**, 022814 (2023).
- [88] Y. Wang, L. M. Sager-Smith, and D. A. Mazziotti, Quantum simulation of bosons with the contracted quantum eigensolver, *New J. Phys.* **25**, 103005 (2023).
- [89] C. L. Benavides-Riveros, Y. Wang, S. Warren, and D. A. Mazziotti, Quantum simulation of excited states from parallel contracted quantum eigensolvers, *New J. Phys.* **26**, 033020 (2024).
- [90] S. Warren, Y. Wang, C. L. Benavides-Riveros, and D. A. Mazziotti, Exact ansatz of fermion-boson systems for a quantum device, arXiv preprint arXiv:2402.12273 10.48550/arXiv.2402.12273 (2024).
- [91] H. Nakatsuji, Equation for the direct determination of the density matrix, *Phys. Rev. A* **14**, 41 (1976).
- [92] D. A. Mazziotti, Exactness of wave functions from two-body exponential transformations in many-body quantum theory, *Phys. Rev. A* **69**, 012507 (2004).
- [93] D. A. Mazziotti, Exact two-body expansion of the many-particle wave function, *Phys. Rev. A* **102**, 030802 (2020), 2010.02191.
- [94] D. A. Mazziotti, Anti-hermitian contracted Schrödinger equation: Direct determination of the two-electron reduced density matrices of many-electron molecules, *Phys. Rev. Lett.* **97**, 143002 (2006).
- [95] D. A. Mazziotti, Anti-Hermitian part of the contracted Schrödinger equation for the direct calculation of two-electron reduced density matrices, *Phys. Rev. A* **75**, 022505 (2007).
- [96] D. A. Mazziotti, Multireference many-electron correlation energies from two-electron reduced density matrices computed by solving the anti-Hermitian contracted Schrödinger equation, *Phys. Rev. A* **76**, 052502 (2007).
- [97] A. E. Rothman, J. J. Foley, and D. A. Mazziotti, Open-shell energies and two-electron reduced density matrices from the anti-Hermitian contracted Schrödinger equation: A spin-coupled approach, *Phys. Rev. A* **80**, 052508 (2009).
- [98] G. Gidofalvi and D. A. Mazziotti, Direct calculation of excited-state electronic energies and two-electron reduced density matrices from the anti-Hermitian contracted Schrödinger equation, *Phys. Rev. A* **80**, 022507 (2009).
- [99] J. W. Snyder and D. A. Mazziotti, Photoexcited conversion of gauche-1,3-butadiene to bicyclobutane via a conical intersection: Energies and reduced density matrices from the anti-Hermitian contracted Schrödinger equation, *J. Chem. Phys.* **135**, 024107 (2011).
- [100] J.-N. Boyn and D. A. Mazziotti, Accurate singlet-triplet gaps in biradicals via the spin averaged anti-Hermitian

- contracted Schrödinger equation, *J. Chem. Phys.* **154**, 134103 (2021), 2104.00626.
- [101] S. E. Smart and D. A. Mazziotti, Efficient two-electron ansatz for benchmarking quantum chemistry on a quantum computer, *Phys. Rev. Res.* **2**, 023048 (2020).
- [102] Z. Hu, R. Xia, and S. Kais, A quantum algorithm for evolving open quantum dynamics on quantum computing devices, *Sci. Rep.* **10**, 3301 (2020), 1904.00910.
- [103] A. W. Schlingens, K. Head-Marsden, L. M. Sager, P. Narang, and D. A. Mazziotti, Quantum Simulation of Open Quantum Systems Using a Unitary Decomposition of Operators, *Phys. Rev. Lett.* **127**, 270503 (2021), 2106.12588.
- [104] IBM-Quantum, <https://quantum-computing.ibm.com/> (2024).
- [105] Qiskit contributors, Qiskit: An open-source framework for quantum computing (2024).
- [106] W. J. Hehre, R. F. Stewart, and J. A. Pople, Self-consistent molecular-orbital methods. i. use of gaussian expansions of slater-type atomic orbitals, *Chem. Phys.* **51**, 2657–2664 (1969).
- [107] Q. Sun, T. C. Berkelbach, N. S. Blunt, G. H. Booth, S. Guo, Z. Li, J. Liu, J. D. McClain, E. R. Sayfutyarova, S. Sharma, S. Wouters, and G. K. Chan, PySCF: the Python-based simulations of chemistry framework, *Wiley Interdiscip. Rev. Comput. Mol. Sci.* **8**, 10.1002/wcms.1340 (2018).
- [108] P. Jordan and E. Wigner, Über das paulische Äquivalenzverbot, *Z. Physik* **47**, 631–651 (1928).
- [109] E. Fradkin, Jordan-wigner transformation for quantum-spin systems in two dimensions and fractional statistics, *Phys. Rev. Lett.* **63**, 322–325 (1989).
- [110] D. P. Craig, Configurational interaction in molecular orbital theory. a higher approximation in the non-empirical method, *Proc. R. Soc. Lond. A Math. Phys. Sci.* **200**, 474–486 (1950).